ECS Transactions, 64 (3) 1039-1048 (2014)
10.1149/06403.1039ecst ©The Electrochemical Society

Low Cost Bipolar Plates for Large Scale PEM Electrolyzers

A. S. Gago, A. S. Ansar, P. Gazdzicki, N. Wagner, J. Arnold, K. A. Friedrich

Institute of Technical Thermodynamics, German Aerospace Center,
Pfaffenwaldring 38-40, Stuttgart 70569, Germany

PEM electrolysis is a promising technology for large scale storage of surplus electricity, though it is still costly mainly due to the manufacture of large area and high purity Ti bipolar plates (BPP). In this work we have developed an Au/Ti coating deposited by electrodeposition/thermal spraying on stainless steel BPP. The coating was physically characterized with SEM and electrochemically evaluated in simulated anode conditions. Interfacial contact resistance (ICR) vs. compaction pressure measurements showed that the coating is highly conductive. It successfully protected the stainless steel substrate from corrosion. However, the Au modification detached after 6 h of application of a potential of 2 V vs. RHE. Consequently the Au modification has to be replaced by either another precious metal or a corrosion resistant electroceramic. The coating reported herein could have a large impact on the cost of PEM electrolyzers for large scale electricity storage from renewables.

1. Introduction

Hydrogen can be used as an energy carrier when produced from renewable energies such as solar or wind by proton exchange membrane water electrolysis (PEMWE) systems (1). PEMWE has recently emerged as the most promising technology for large H_2 production from surplus renewable electricity thanks to its rapid response under dynamic operation and high specific energy density (2). Main priorities for the large scale H_2 production are high capacity, long lifetime and cost reduction. In this sense, key components of PEMWE that determine largely the stack cost are the stack bipolar plates (BPP) or separators (3,4). The high cost of the BBP is due to the following:

1. The use of high purity titanium as base material.
2. Machining process of flow fields on titanium which is complicated and costly (5).
3. The need of coatings on titanium for reducing anodization (6). The oxide layer that is formed on the surface of the metal under high potentials in acid medium increases the ohmic resistance (7,8), limiting the durability of the stack.

A more suitable material for bipolar plates would be stainless steel, which is cheaper and easier to machine than Ti. However, this non-noble metal corrodes dramatically when used in the anode of a PEMWE stack. Furthermore, the ions released from the corrosion process poison the catalysts coated membrane (CCM) of the electrolyzer (9). Consequently, stainless steel has to be protected with a coating that is corrosion resistant in acid environment and conductive at the same time.

There is an extensive amount of literature on coatings for stainless steel BPP of proton exchange membrane fuel cells (PEMFC) (10-12). However there are no reports that similar coatings can be used in the PEMWE environment. In this work we report the development and evaluation of an Au/Ti coating for stainless steel bipolar plates of PEM electrolyzers. It was deposited on the substrate by successive steps of vacuum plasma spraying (VPS) and electrodeposition of Ti and Au, respectively. Subsequently, the bilayer coating was physically and electrochemically characterized in simulated conditions of PEMWE.

2. Experimental

2.1 Coating development

Titanium coatings were deposited on sandblasted stainless steel (ss) plates (47 x 47 x 1 mm^3) made of Crofer® 22 H by VPS. The substrate was pre-heated up to 250 °C. Several parameters such as type of plasma torch nozzle, powder feeding rate, and plasma gas flow rates of Ar, N_2 and H_2 were carefully chosen to achieve a plasma enthalpy (*h*) of 21.3 MJ kg^{-1}. A torch sweep rate of 500 mm s^{-1} was used. Grade 1 (Gd1, grain size < 45 µm) Titanium powder with a from TLS Technik Spezialpulver (Germany) was sprayed in a VPS system at a chamber pressure of 50 mbar to prevent the presence of O_2 from the air and thus forming of TiO_2, which reduces the electrical conductivity of the coating. Four layers of Ti coating were thermally sprayed on the stainless steel substrates. Thereafter, a coating of Au, termed surface modification, was deposited on the Ti back layer by electrodeposition technique. For this purpose an acidic (pH = 1.5) potasium-dicyanoaurat (I) ($K[Au(CN)_2]$) solution was used as source of Au. The content of potassium-dicyanoaurat was 2.95 g (68,2%) per liter. The plating was performed galvanostatically with 70 mA cm^{-2} for 8 minutes. During this time about 0.53 mg/cm^2 of Au were deposited on the Ti coating. The measurement of average thickness and roughness of the Au/Ti coating was carried out using digital image analysis.

2.2 Physical characterization

Cross section and topographic images of the Au/Ti coatings before and after corrosion measurements were taken with a SEM Zeiss ULTRA plus with charge compensation. The accelerating voltage was 15 kV with a working distance of 8.4 mm and the back-scattered electrons detector was used. Interfacial contact resistance (ICR) measurements were carried out following the method reported elsewhere (13,14). In short, samples Au/Ti/ss were placed between two pieces of Toray GDL paper. This "sandwich" like arrangement was compressed between two Cu cylinders by means of a hydraulic press. Prior to every measurement the surface of the cylinders in contact with the Toray paper was cleaned with diluted H_2SO_4. The positive and negative terminals of a power supply were connected to the Cu cylinders. An electrical current of 5 DCA was applied between the Cu terminals and the voltage difference was measured for various compaction pressures. The ICR between the Toray GDL and the coating was determined using an equivalent electrical circuit.

2.3 Corrosion evaluation

Electrochemical measurements were performed using an Autolab PGSTAT12 Potentiostat/Galvanostat and a three-electrode cell containing about 1l of 0.5 M H_2SO_4 heated at 65 ºC. Prior to the measurements the electrolyte was saturated for 20 min with high purity O_2 (Praxair) to simulate the PEMWE anode environment. A platinum foil and a reversible hydrogen electrode (RHE) from HydroFlex® were used as counter (CE) and reference electrode (RE), respectively. As working electrode (WE) a sample holder was manufactured in Polyether ether ketone (PEEK) and squared coated samples of 18 x 18 mm^2 were tightly fixed with a cap and a silicone O-ring. This cap had a 1 cm^2 hole and another O-ring that allowed exposing this area to the electrolyte while keeping the rest of the coating dry. Figure 1a shows a scheme of an Au/Ti/ss sample indicating the corrosion evaluation zone delimited by the hole in the cap. Figure 1b shows a photo of the Au/Ti/ss sample in the electrode holder, immersed in the hot electrolyte solution.

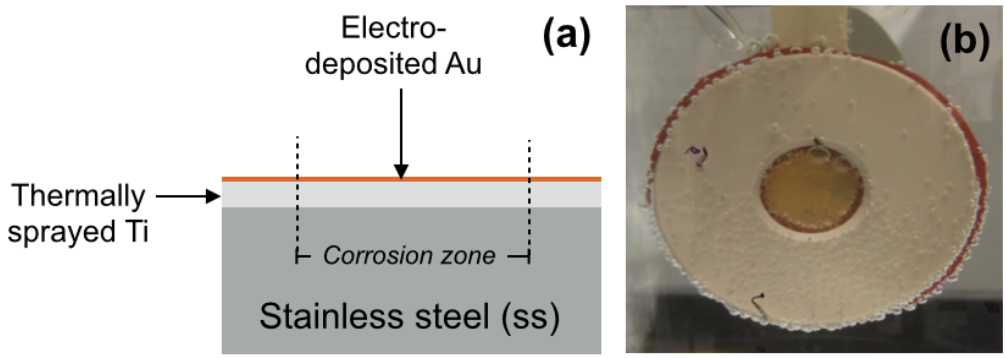

Figure 1. (a) Scheme of the Au/Ti coated ss samples indicating the target surface for testing and analysis. (b) Front view image of the WE sample holder with the coated sample immersed in O_2-saturated 0.5 M H_2SO_4 electrolyte used for the corrosion measurements.

A stainless steel BPP with a 20 cm^2 active surface area was coated in order to evaluate the protection of the layer on edges and irregular 3D areas. The BPP had a pillar-type flow field design similar to those used in direct methanol fuel cells (DMFC). Figure 2 shows photos of the BPPs made of (a) Ti, (b) ss and (c) Au/Ti/ss. The BPP were immersed in 5 mM H_2SO_4 at 24 °C and constantly polarized at +2.5 DCV for 6 hours. A coated plate of the same material of the BPP served as cathode. The iron content of the solution was measured at the end of the experiment, using a HI721 Iron Checker from HANNA instruments.

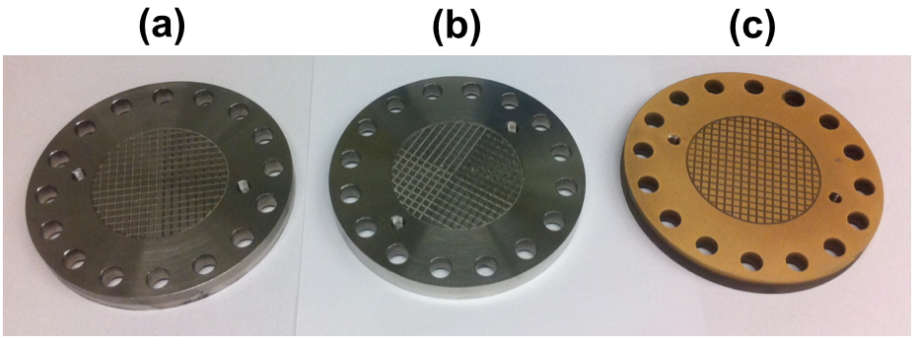

Figure 2. Images of PEMWE bipolar plates made of (a) Ti, (b) stainless steel (ss) and (c) Au/Ti coated ss prior to the corrosion tests.

3. Results and discussion

3.1 SEM analysis

The thermally sprayed Ti coating has an average thickness of 30.8 µm and produced a leak rate 8.6 mbar l cm^{-2} s^{-1}. It is possible to produce a denser layer with a lower leak rate by lowering the torch sweep rate from 500 to 350 mm s^{-1} (15), but then the roughness property of the coating is compromised. As will be explained later, the high roughness of the Ti coating is mainly responsible for the good adherence of the Au coating on Ti and high conductivity.

Scanning electron microscopy (SEM) analysis was carried out on Au/Ti/ss in order to study the morphology and determine the negative effects of corrosion at high potentials. Figure 3 shows a cross section SEM image of the thermally sprayed Ti coating having a thin layer of Au (bright) deposited on its surface, (a, c) before and (b, d) after corrosion measurements. First of all, the SEM image shows that the spherical Ti Gd1 particles where completely melted during the VPS deposition process leading to a highly dense Ti coating. Secondly the coating has a roughness factor of about 0.62, which was calculated from the ratio between the real surface area and the geometric surface area of the sample. This property of the thermally sprayed Ti coating allows improving the adherence of the Au layer on its surface, which eventually will prevent further anodization during operation of the PEM electrolyzer. In fact, the Au coating does not adhere at all on a polished surface of Ti, as a nanolayer of TiO_2 forms between the two metals due to passivation of Ti.

Figure 3b shows a cross section SEM image of the Au/Ti coating after corrosion tests. As can be observed the Au layer on the surface of the Ti coating has been practically detached during the electrochemical measurements. Conversely the Ti layer has effectively protected the stainless steel substrate and neither pinholes nor pitting corrosion was observed. A topographic SEM image of the Au/Ti coating deposited on stainless steel, before corrosion measurements, is shown in Figure 3c. As can be seen the Au nanoparticles cover most of the irregular surface of the Ti coating. However, Figure 3d shows again that layer of Au has been almost completely removed from the surface of Ti.

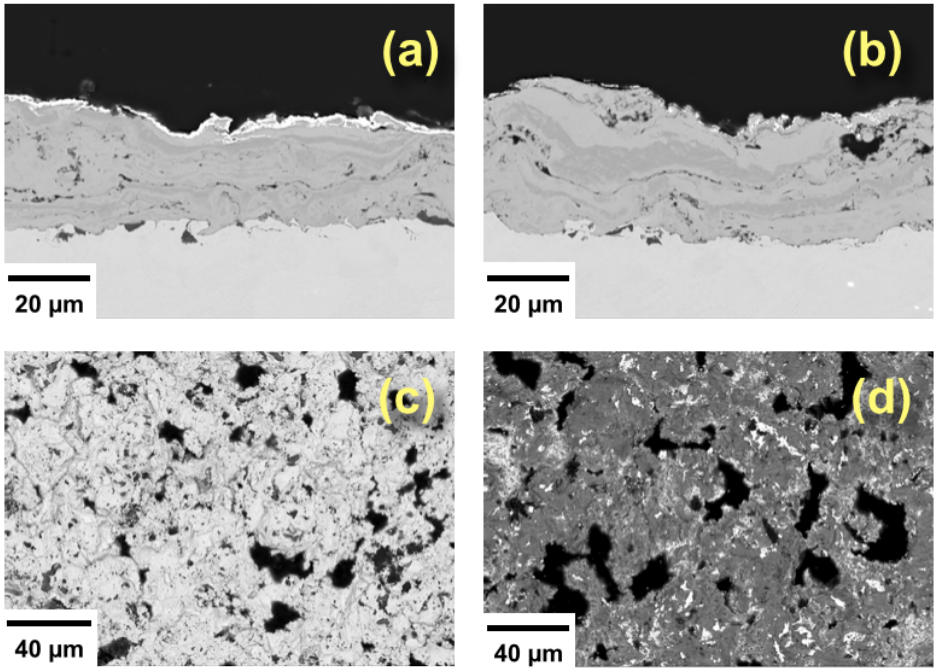

Figure 3. SEM cross section and topography images of Au/Ti coated ss samples (a, c) before and (b, d) after corrosion measurements.

Additional work involving spectroscopic techniques such EDS, XPS and XRD is currently being carried out to find more about the microstructure of the Au/Ti. The results will be published in a separate report.

3.2 Interfacial contact resistance (ICR) measurements

The first requirement for BBP of PEM electrolyzers is a high through-plane electrical conductivity or rather low interfacial contact resistance (ICR). This parameter determines the electrical contact of the BPP with the current collector or GDL. This requirement applies to BPPs made of either Ti or stainless steel. The ICR measurements with respect to the compaction pressure on finely sanded Ti/ss and rough Au/Ti/ss samples are shown in Figure 4. At a compaction force of 150 N cm^{-2} an area resistance of 403 mΩ cm^2 was measured for the Ti/ss sample, which is a value expected for a passivated Ti surface. Even at 605 N cm^{-2} the ICR only decreases down to 55 mΩ cm^2. In contrast the ICR of the Au/Ti/ss samples is less than 10 mΩ cm^2 at 150 N cm^{-2}. Measurements were repeated using a new piece of Toray paper in between the Cu cylinder and the Au/Ti coating. The obtained results lay within the experimental error, indicating that the through-plane conductivity of the coating is not affected the effect of compressing it against the carbon GDL.

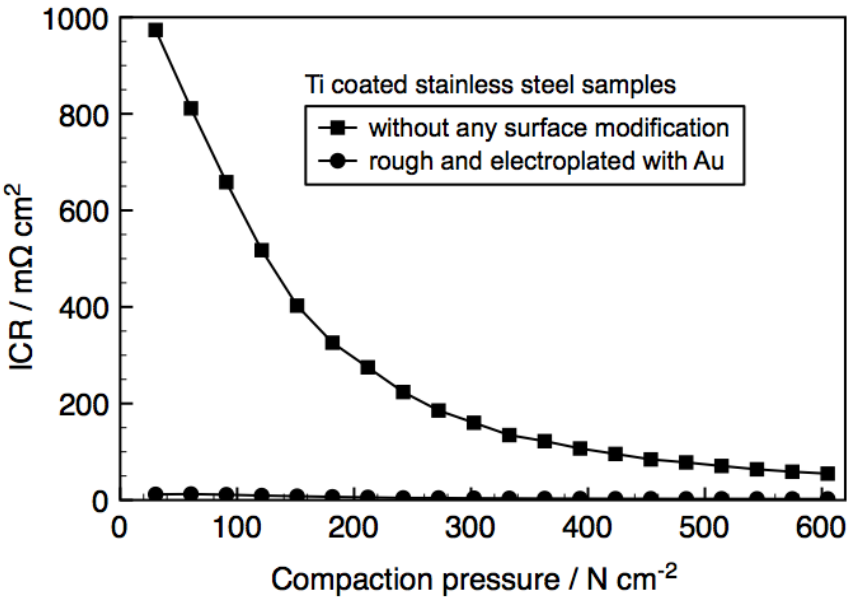

Figure 4. Interfacial contact resistance (IRC) vs. compaction pressure of unmodified and Au-modified Ti coated stainless steel samples.

The surface modification of the Ti coating by Au has a very positive effect as passivation is halted. Indeed the growth of the TiO_2 layer on Ti BPP increases the ohmic resistance of the PEMWE stack, limiting its durability. It has been reported that the performance of unitized regenerative fuel cells (URFC) is greatly improved when the surface of the Ti BPP is modified with Au (16) or Pt (17).

Finally, the ICR after corrosion tests was not measured as it is obvious from Figure 3d that the surface modification with Au is not effective anymore. In this sense the choice of Au is not adequate. As alternative, other precious metals such as Pt, Ir or a corrosion resistant electro-ceramic like $Ti_{1-x}W_xO_2$ (18) can substitute Au.

3.3 Corrosion tests

The second most important requirement of BBP of PEM electrolyzers is corrosion resistance in acid environment at high anodic potentials. This requirement applies to either Ti or any coated substrate such as stainless steel. In order to evaluate the corrosion resistance, a potential of 2 V vs. RHE was applied to the coated stainless steel samples, as this is a normal operating condition of a PEMWE. In contrast coated BPP materials of PEMFC are usually evaluated only up to 0.82 V vs. RHE (19, 20).

Figure 5 shows the potentiodynamic polarization characteristics of coated stainless steel samples recorded before (scan 1 and 2) and after the chronoamperometric test, which was carried out at 2 V vs. RHE in O_2-saturated H_2SO_4 at 65 °C. These experimental conditions simulate and accelerate the corrosion degradation of the investigated materials. The electrochemical results from this test are shown in the inset of Figure 5. Uncoated stainless steel (dashed line) was included as well for comparison purposes.

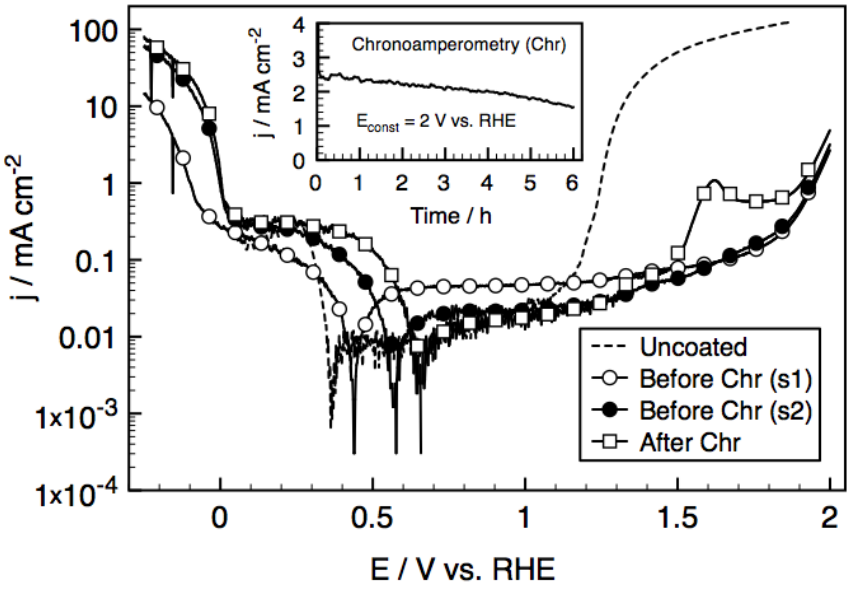

Figure 5. Potentiodynamic polarization curves of coated stainless steel samples recorded before (scan 1 and 2) and after the chronoamperometric test. The inset shows such test which was carried out at a constant potential of 2 V vs. RHE. Uncoated stainless steel (dashed line) was included as well for comparison purposes. Measurements were carried out in O_2-saturated 0.5 M H_2SO_4 at 65 °C.

Table I groups some electrochemical parameters extracted from Figure 5. The polarization resistance (R_p) was calculated using the following equation

$$R_p = \frac{\beta_a \beta_c}{2.3 j_{corr}(\beta_a + \beta_c)} \quad [1]$$

where ß$_a$, ß$_c$, j_{corr}, and R_p are the Tafel slopes of the anodic and cathodic reactions, the corrosion current density, and polarization resistance, respectively.

TABLE I. Electrochemical parameters: corrosion potential (E_{corr}); corrosion current (i_{corr}); anode (β_a) and cathode (β_c) Tafel slopes and polarization resistance (R_p) of the coated stainless steel before (scan 1 and 2) and after the chronoamperometric (chr) test.

Coated stainless steel	E_{corr} / V vs. RHE	j_{corr} / µA cm^{-2}	β_a / mV dec^{-1}	β_c / mV dec^{-1}	R_p / x 10^3 Ω
Before chr (s1)	0.44	4.76	63	91	3.40
Before chr (s2)	0.57	1.52	36	35	5.08
After chr	0.66	3.82	148	61	4.92

It can be observed that the corrosion potential (E_{corr}) increases after the prolonged application of high potentials as a result of the mixed potential between oxygen reduction reaction (ORR) on Au and the passivation of the Ti back layer. The j_{corr} and R_p parameters are mainly dominated by the high roughness of the bilayer coating. Moreover, a high anodic Tafel slope β_a, which is symptomatic of anodized Ti, was calculated after

the chronoamperometric test. As shown in Figure 3d the Au modification detached almost completely after the chronoamperometric experiment. In order to explain this negative result, the electrochemistry of Au, which has been widely studied (21), should be recalled. Thermodynamically a multilayer of $Au(OH)_3$ or $Au_2O_3 \cdot 3H_2O$ is readily produced at 1.46 V (pH = 0) on the surface of Au. The oxidation of Au can be observed at slightly higher potentials in the curve labeled "After Chr" in Figure 5. The growth of amorphous $Au(OH)_3$ is hindered by a monolayer oxide film which passivates the surface in regard to the hydrous Au. At 2 V the oxygen evolution reaction (OER) occurs as some of the monolayer oxide material is converted to gold peroxide species which decomposes yielding to oxygen gas. Both the oxygen gas evolution and hydrous oxide growth may involve formation of unstable AuO_2 species. This phenomenon along with the increasing corrosion of Ti and TiO_2 might lead to the detachment of the Au nanoparticles

The most interesting observation that can be made from Figure 5 is that corrosion of the stainless steel substrate could not be detected at all, either before, or after the chronoamperometric test. A concomitant increase in the current density in the transpassive region of the metal is characteristic of its dissolution in acid media. Such anodic current was not measured at all in the coated samples.

Cross-section images of a coated stainless steel BBP (not shown in this work) revealed that the coating covers all the regions of the manifolds, the exposed 3D areas of the flow field, inlet/outlet holes, edges, corners and even some regions of the backside of the BPP. A corrosion test was carried out on a Au/Ti coated stainless steel BPP in order to test the effectiveness of the coating deposition process on areas with irregular shape. In this case the experimental conditions were 5 mM H_2SO_4, at 24 °C, under an applied potential of +2.5 VDC. The concentration of Fe^{2+} in the acidic solution was measured at the end of the experiment and it turned to be around 0 ppm or rather below the detection limit of the device. The same experiment was performed on an uncoated BPP. After 6 hours of constant anodic polarization on the uncoated BPP, the $[Fe^{2+}]$ in the electrolyte was ca. 3.8 ppm. In addition, the color of the acid solution turned from transparent to yellow due to the Cr^{3+} released as result of galvanic corrosion of the substrate.

Finally, the coating deposition techniques discussed herein are very suitable for protecting large area BPP of PEMWE and the production cost of the plates that are currently being used is greatly reduced. An estimation (not shown in this work) of the cost of coating BPP for electrolyzers in the Megawatt range was calculated. Roughly 25 or more (high volume) BPP of 32 cm high x 32 cm long x 0.1 cm thick would be 2.3 € / piece. The surface modification with Au or other precious metal is not included in this calculation.

4. Conclusions

In this work the development, physical and electrochemical characterization of a coating for large scale bipolar plates (BPP) of PEM electrolyzers was reported. This coating was produced by successive steps of vacuum thermal spraying (VPS) of Ti and electrodeposition of Au. The Au/Ti coating has an average thickness of 30.8 µm and a roughness factor of 0.64. This later property is quite advantageous for the adhesion of the Au nanoparticles on the Ti layer and thus reducing the interfacial contact resistance

(ICR). The measured (ICR) was lower than 10 mΩ cm^2 at 150 N cm^{-2}. The coating was evaluated in an oxidative environment under high potentials, which simulate anodic environment of the electrolyzer. The back coating of Ti protected the stainless steel substrate from corrosion over an extended period of time. However, the Au modification was detached after 6 h at 2 V vs. RHE. The thermal spraying technique allows producing dense and robust Ti layers that offer the required corrosion protection to stainless steel BPP of PEM electrolyzers. However the surface of this coating has to be modified in order to avoid the formation of TiO_2. Finally, the techniques used for producing the coating presented herein can be easily set up for industrial production of low cost BPP for large scale PEM electrolyzers.

Acknowledgments

The authors acknowledge the German *Bundes-ministeriums für Bildung und Forschung* (BMBF) for financial support in the project No. 0325440A. The authors are gratefully to Günter Roth, Gudrun Steinhilber and Ina Plock for spraying the VPS coatings, the preparation of the samples and the SEM images, respectively. Finally, we thank to Thomas Kupke for manufacturing the sample holder.

References

1. Fuel Cell Today survey: *Water Electrolysis & Renewable Energy Systems*, http://www.fuelcelltoday.com/analysis/surveys/2013/water-electrolysis-renewable-energy-systems, (2013).
2. K. E. Ayers, L. Moulthrop, and E. B. Anderson, *ECS Trans.*, **41**(46), 75–83 (2012).
3. E. T. Ojong, E. Mayousse, T. Smolinka, and N. Guillet in *TECHNOPORT RERC 2012*, Hydrogen Session – Bipolar plates for PEM fuel cells and electrolyzers, Trondheim, Germany, April 16 - 18, 1–19 (2012).
4. K. E. Ayers, C. Capuano, and E. B. Anderson, *ECS Trans.*, **41**(10), 15–22 (2012).
5. H. G. Kim, L. K. Kwac, and W. Han in *Lecture Notes in Information Technology* Vol. 13, p. 373 - 379, International Conference on Power and Energy Systems (2012).
6. J. T. Wang, C. Wang, and Z. Q. Mao, *Int. J. Hydrogen Energy*, **37**, 12069–12073 (2012).
7. H. Y. Jung, S. Y. Huang, and B. N. Popov, *J. Power Sources*, **195**, 1950–1956 (2010).
8. H. Y. Jung, S. Y. Huang, P. Ganesan, and B. N. Popov, *J. Power Sources*, **194**, 972–975 (2009).
9. F. Andolfatto, R. Durand, A. Michas, P. Millet, and P. Stevens, *Int. J. Hydrogen Energy*, **19**, 421–427 (1994).
10. M. C. L. de Oliveira, G. Ett, and R. A. Antunes, *J. Power Sources*, **206**, 3–13 (2012).
11. R. A. Antunes, M. C. L. Oliveira, G. Ett, and V. Ett, *Int. J. Hydrogen Energy*, **35**, 3632–3647 (2010).
12. S. Karimi, N. Fraser, B. Roberts, and F. R. Foulkes, *Adv. in Mater. Science and Engineering*, **2012**, 1–22 (2012).

13. H. Wang, M. A. Sweikart, and J. A. Turner, *J. Power Sources*, **115**, 243–251 (2003).
14. U. F. C. Council, *Electrical Conductivity Testing Protocols Task Force Materials & Components Working Group*, Document No. 05–160 (2004).
15. A. S. Gago, A. S. Ansar, N. Wagner, J. Arnold, and K. A. Friedrich, in *Proceedings of the 4th European PEFC and H_2 Forum*, Chapter 6, Session A07 – p. 11-18, Lucerne Switzerland (2013).
16. H. Y. Jung, S.-Y. Huang, P. Ganesan, and B. N. Popov, *J. Power Sources*, **194**, 972–975 (2009).
17. H. Y. Jung, S.-Y. Huang, and B. N. Popov, *J. Power Sources*, **195**, 1950–1956 (2010).
18. G. Abadias, A. Gago, and N. Alonso-Vante, *Surf. Coat. Technol.*, *205*, S265–S270 (2011).
19. Y. Wang and D. O. Northwood, *J. Power Sources*, **191**, 483–488 (2009).
20. L Wang, D. O. Northwood, X. Nie, J. Housden, E. Spain, A. Leyland, and A. Matthews, *J. Power Sources*, **195**, 3814–3821 (2010).
21. L. D. Burke and P. F. Nugent, *Gold Bull.*, **30**, 43–53 (1997).